

# **Ziggurat Journal of Materials Technology (ZIMT)**

(ISSN 2633-3155 online)





Article

# Osseointegration of Cylindrical Zirconia–Alumina Functionally Graded materials, Dental implant by Electrophoretic Deposition

Awham J. Salman<sup>1,\*</sup> , Nada M. H. Al-Ghaban<sup>2</sup>, Mohammed J. Eesa<sup>3</sup>, Alaa A. Atiyah<sup>4</sup>, Saad B. H. Farid<sup>4</sup>

- <sup>1</sup>Technical College, Al-Mussaib, Al-Furat Al-Awsat Technical University, Iraq
- <sup>2</sup>College of Dentistry, University of Baghdad, Iraq
- <sup>3</sup>College of Veterinary Medicine, University of Baghdad, Iraq
- <sup>4</sup>Department of Materials Engineering, University of Technology Iraq, Baghdad, 10066, Iraq
- \* Corresponding Author, email: awhamj@atu.edu.iq

DOI: 10.36533/zjmt.v1i1.1

#### ARTICLE INFORMATION

Article History
Received: 14 April 2020
Revised: 29 June 2020
Accepted: 30 July 2020
Published: 11 November 2020

Keywords
Electrophoretic deposition
Graded materials
Suspension parameters
Applied potential
Histological test

#### **ABSTRACT**

Electrophoretic deposition (EPD) technique is used to prepare zirconia-alumina composite layers based on the principle of functionally graded materials (FGM). The FGM were prepared with five layers. The outer layer was composed of pure  $\alpha$ -alumina to promote biocompatibility while the inner layer was stabilised zirconia (3Y-TZP), to benefit from its tough properties. The intermediate layers were stepwise graded layers. The stability of the EPD suspensions was the main challenge during the preparation steps. Due to availability and low cost, alcoholic solutions of polyethylene glycol (PEG) and toluene were used to control conductivity, dielectric constant and the viscosity of the suspension. The appropriately applied potential,  $(\zeta)$ , for the deposition of each layer, was achieved via gradation of the applied voltage, which was to optimise the packing of each layer and avoid cracking after sintering at 1500 °C. The cylindrical-shaped green specimens were obtained via deposition on graphite electrodes. A small amount of acetic acid was added during the deposition of the final outer alumina layer to introduce porosity, via the bubbling of acetic acid, to encourage osseointegration. The sintered specimens were implanted in rabbit tibial bone. In vivo histological tests showed the successful osseointegration of the implants to the rabbit bone.

## 1. Introduction

The replacement of the tooth root with an implant into the jaw is an essential step for whole tooth replacement; the implant is then capped with a ceramic or polymeric dental crown. A whole denture or bridge can also be attached to the implant. The dental implant carries various loads during mastication and needs to be examined for its mechanical properties, biocompatibility and integration with the bone. For these purposes, different materials, shapes and surface characteristics were examined to improve clinical outcomes. Titanium metal and its alloys have been used for dental implants since the 1960s and there have been numerous designs so that mechanical fixation to the bone is continuously improved. Surface modification of titanium alloys is usually performed to improve biocompatibility with the jawbone. However, this biocompatibility is limited by the generation of thin fibrous tissue that assists mechanical interlocking with the bone. The limited biocompatibility, cost and the complicated fabrication process of titanium alloys encourage the use of ceramic implants [1-3].

Alumina, zirconia, zirconia-toughened alumina and alumina/zirconia composite are used as dental implants. The term 'zirconia' is used for stabilised zirconia in the literature of dental materials; usually yttria-tetragonal zirconia particles (Y-TZP) with various yttria content (8, 5 and 3 mole%). These materials are known for their superior mechanical properties and biocompatibility. Alumina was frequently used in the 1980s with zirconia being used from the early 1990s. Afterwards, studies of zirconia-toughened alumina and alumina/zirconia composite dental materials appeared. Different shape-forming techniques and sintering procedures were used to attain smooth surfaces and better compression strengths of the final product [4-12]. However, surface porosity and/or surface roughness are required to ensure osseointegration (mechanical interlocking) with the jawbone. Additionally, surface porosity and roughness encourage the formation of blood vessels that encourage osseoinduction (growth of local bone). Alumina and zirconia are both utilised as dental implants due to their biocompatibility, although zirconia has higher mechanical properties. However, the alumina implant is preferred because it is more hypoallergenic (unlikely to cause an allergic reaction) compared to zirconia [13-17].

Dental implants based on the alumina/zirconia layered composite appear to satisfy two requirements. The first is to utilise the mechanical properties of zirconia as inner layers. The second is to make use of better biocompatibility of alumina as an outer layer. However, the difference in sintering shrinkage and the thermal expansion between alumina and zirconia introduces harmful cracks and the separation of layers. To overcome these difficulties, the concept of functionally graded materials (FGM) was generated and graded alumina/zirconia layer composites were developed. The inner layer is composed of 100% zirconia and the content of alumina is gradually increased in successive layers ending with 100% at the outer layer. Several techniques are used for the fabrication of FGM, as shown in review articles [18-20]. However, the EPD, which is the electrodeposition of nonconductive powder suspension, that relies on the surface charge of the particles has emerged as a superior shape-forming technique. The EPD process provides better control of the composition, thickness, uniformity, gradation profile, the final shape and residual stresses after sintering the deposited FGM [21-25]. The EPD technique for the synthesis of FGM dental implants also provides better control of surface characteristics, such as roughness and open porosity. Controlling these parameters enhances the osseointegration of the implant to the bone. EPD also facilitates the introduction of other reinforcement phases like SiC, carbon nanotubes and hydroxyapatite to meet the specific needs of patients according to age and the location of the implant. The utilisation of nanomaterials greatly assists the successful control of the EPD process of biomaterials, particularly alumina and zirconia [26-29]. The failure of dental implants is rare; however, failure is typically a consequence of infection or poor osseointegration that leads to rejection or bone loss. Thus, to claim a newly developed material as a successful dental implant, a range of biocompatibility tests was designed to ensure safe osseointegration of the implant to the bone. The most extensive test is the histomorphometric test that evaluates bone microarchitecture, metabolism and remodelling (i.e. reconstruction) after implantation. The rabbit tibial bone is a suitable model to test biocompatibility and host/implant response and assess bone healing around different implant surfaces [30-34]. In this work, a multilayered FGM of zirconia-alumina cylindrical implant was prepared by EPD. A unique set of suspension solutions and applied voltage profiles was devised to obtain the green parts. Each separate layer, in addition to the sintered FGM dental implant, was subjected to characterisations. Finally, implantations on rabbit tibial bone were performed and histomorphometric tests were conducted three and six weeks after implantation.

# 2. Materials and Methods

# 2.1 Electrophoretic deposition process

Table (1) presents the starting materials used in the EPD process, including the suspended powders and components of the suspension liquid. The alumina and zirconia powders were subjected to particle size analysis (90 plus Laser Particle Size Analyzer, located at the University of Technology/Nanotechnology and Advanced Materials Research Centre). The EPD process was performed using an HT power supply (EISCO, AC-DC max 400V) applying various DC voltages. Graphite cylinders were used as electrodes. The EPD process was used to fabricate zirconia–alumina high-order FGM (5-layers). Table 2 shows the composition of vol.% of each layer. A PEG ethanol solution was utilised as a suspension solution. Toluene was also added to the powder suspension of the first and second layers. The important physical properties of ethanol, PEG [35] and toluene [36] for the EPD process are listed in Table 3. Numerous experiments were performed to obtain the best set of suspension properties (viscosity and dielectric constant) that allowed reasonable deposition time and high-green density. An amount of acetic acid was included when the outer layer of 100% alumina was deposited. This was to enable the released gasses at the surface to create the required porosity at the surface. The final amounts of the suspension components are listed in Table 4. The table also lists the value of the applied DC voltage that controlled the potential ( $\zeta$ ) of the EPD process.

In the beginning, each layer was deposited separately for X-ray diffraction (XRD) and scanning electron microscopy (SEM) characterisations. Then, complete FGM parts were produced for sintering and implantation. XRD characterisations were carried out using a programmable X-ray diffractometer (XRD-6000, NF, located at the

University of Technology/Nanotechnology and Advanced Materials Research Centre) with Cu  $K_{\alpha 1}$  in the  $2\theta$  range of 5–100 degrees. FGM sintering was performed using a high-temperature programmable furnace (HUMONLAB, Germany, located at the University of Babylon, College of Materials Engineering). The heating ramp was 5 °C/min; max temperature 1500 °C; holding time 2.5 hrs. The sintered parts were then left for furnace cooling (about 10 °C/min). Microstructural observations of the sintered parts were carried out using SEM (Inspect S50 scanning electron microscope, located at the University of Al-Nahrain, College of Science). Line scan energy dispersive X-ray (EDX) was also performed (TESCAN, Vega III Czech Republic, located at the laboratory of nanotechnology, Ministry of Science and Technology) at the cross-section of the sintered part to obtain the final chemical composition of each layer. The SEM and EDX tests were conducted from the inner layer to the outer layer, as seen in Figure 1. Finally, compressive strength was measured by a universal testing machine (Type WDW-50, located at the University of Technology, Department of Materials Engineering).

## 2.2 Implantation and histological test

After the fabrication and characterisation of the zirconia-alumina FGM via the EPD process, the FGM parts were ready for *in vivo* implantation, followed by evaluation of the implants by histological test. Conventional *in vivo* implantation on the rabbit tibial bone, as the host bone, was performed in the surgical room of the College of Veterinary Medicine, which was equipped with the necessary surgical materials and instruments. The hard (bone) tissue and the implant hard-tissue interface were monitored at time intervals of three and six weeks. A team of two medical doctors (MDs) and one lab expert (medical lab analysis) were involved in this work, monitored by the materials engineer. The implants and surgical instruments were sterilised. Rabbits aged 10-12 months old were sacrificed. They were kept in separate cages, had free access to tap water and were fed with standard pellets. They were left for two weeks in the same environment before the surgical operation. Surgery was performed under sterile conditions with a gentle surgical technique. An incision was made on the medial side of the legs, about 3 cm in length, to expose the tibial bone of the rabbit. The skin, fascia and periosteum (vascular connective tissue) were carefully reflected. Drilling was done using a round bur with intermittent pressure. The hole was enlarged gradually with a drill of 3.2 mm, as seen in Figure 2a. The implant was placed in the hole with slight pressure at 6 mm and completely introduced into the bone (Figure 2b). The histological tests started with bone-sectioning performed by a disc cutter on a low rotating speed and vigorous cooling, while the animal was anaesthetized with an overdose (lethal dose) of medication. The bone-implant blocks were immediately stored in 10% of freshly prepared formalin and left in for one day. Conventional sample preparation was performed to extract the organic materials from the bone-implant blocks. The test sample only contained the hard (bone) tissue and the implant. Thin sectioning of the samples (4 µm thickness) was performed with a microtome followed by drying the slices (sections). Haematoxylin (violet fluorescent dye) and eosin (red fluorescent dye) were used to stain the hard tissue to facilitate microscopic examination; this is also known as H&E staining. Microscopic examinations were carried out via a stereo optical microscope for each slice. Finally, the resultant photographs were subject to histological analysis.

Table 1: The starting materials for the EPD process

Material	Formula	Purity	Origin	
α-Alumina	Al203	99	China	
3Y-TZP	$ZrO_2$	94.2	China	
Ethanol	C <sub>2</sub> H <sub>5</sub> OH	99.9	99.9 Spain	
Toluene	$C_6H_5CH_3$	99.9	Germany	
Polyethylene glycol	H(OCH <sub>2</sub> CH <sub>2</sub> )nOH	99.8	China	
PEG	MW=4000	99.0	Cillia	
Acetic acid CH <sub>3</sub> COOH		99.7	Britain	

Table 2: The composition profile of the FGM layers

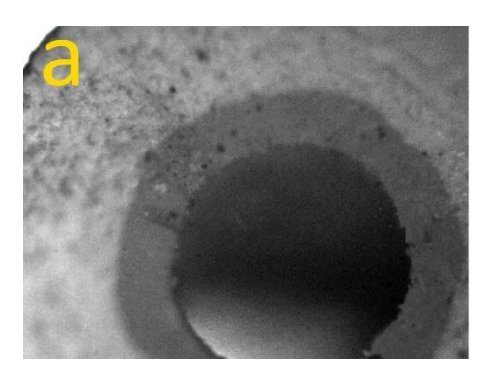
Solution no.	Commercial or could be considered as a second of the commercial or could be considered as a second or considered as a seco			
Inner to outer layer	Composition vol.% of the suspended powder			
First	100 vol.% ZrO <sub>2</sub>			
Second	75 vol.% ZrO <sub>2</sub> + 25 vol.% Al <sub>2</sub> O <sub>3</sub>			
Third	50 vol.% ZrO <sub>2</sub> + 50 vol.% Al <sub>2</sub> O <sub>3</sub>			
Fourth	25 vol.% ZrO <sub>2</sub> + 75 vol.% Al <sub>2</sub> O <sub>3</sub>			
Fifth	100 vol.% Al <sub>2</sub> O <sub>3</sub>			

Table 3: The physical properties of the suspension solution components [35, 36]

Material	Viscosity [cP] 10 <sup>-3</sup> N.s.m-2	Relative dielectric constant	
Ethanol	1.0885	24.55	
PEG	16.265	37.7	
Toluene	0.59	2.38	

Table 4: The composition of 25 ml suspension for each layer

Solution no. Inner to outer layer	ZrO <sub>2</sub> [g]	Al <sub>2</sub> O <sub>3</sub> [g]	PEG [g]	Ethanol [ml]	Toluene [ml]	Acetic acid [ml]	Applied potential (ζ)
First	0.5	-	0.38	22.5	2.5	-	250
Second	0.40	0.1	0.38	22.5	2.5	-	260
Third	0.29	0.21	0.3	25	-	-	270
Fourth	0.16	0.34	0.25	25	-	-	280
Fifth	-	0.5	0.25	25	-	1.5	290



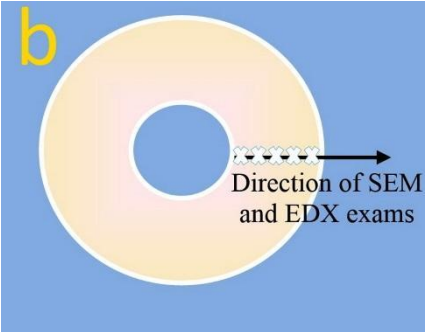


Figure 1: (a) Cross-section of depositing part; (b) Direction of examination



Figure 2: (a) The bone hole; (b) Insertion of the implant

# 3. Results and discussion

The measured diameters of the alumina and zirconia powders were 4.0 NM and 2.4 NM, respectively. Thus, separation of alumina from zirconia in the suspension was not expected during the deposition time (2 min for each layer). Ethanol-dissolved PEG was used as a suspension solution for the first time for the deposition of zirconia-alumina FGM, utilising its long polymer chains (MW=4000) to suspend high-density powders of zirconia and alumina. PEG was previously used with EPD solutions, such as isopropanol and other materials, such as hydroxyapatite and graphene [37, 38].

Experimentation revealed that the green density of the 100% zirconia and 75% zirconia layers were higher in suspensions containing toluene. This may be attributed to the fact that zirconia has a higher dielectric constant compared to alumina [39]. For this reason, toluene was added to the suspensions accompanied by the deposition of 100% zirconia and 75% zirconia layers (Table 4) to compensate the dielectric constant as the dielectric constant of toluene is much lower than ethanol (Table 3).

The applied voltage was varied for successive layers (Table 4) to compensate for the reduction in conductivity of the suspension proportional to the thickness of the deposit. The green density of the deposited FGM was 1.94g. Cm<sup>-3</sup> and the outer diameter was 3.6 mm. The inner diameter is that of the graphite electrode diameter (1.3 mm).

After sintering the deposited FGM, the graphite electrode was burned without ash. The final thickness of the five layers was 0.95 mm and the outer diameter was 3.2 mm. Figure 3 shows an optical image of the sintered FGM. The figure shows no evidence of cracks or separation of layers after sintering that indicate a suitable gradation of zirconia–alumina layers. The zirconia–alumina gradation of a cross-section of the sintered FGM is shown in Figure 4. The figure shows a stepwise gradation of FGM layers with smooth interfaces and without a sign of the layers separating. The gradation of the composition is also shown clearly via an EDX line scan (Figure 5) for the polished cross-section plane of the sintered FGM. In this figure, the Zr element is monitored for zirconia and the Al element is monitored for alumina.

Figure 6 shows the difference in the roughness of the outer alumina surface in cases with and without the addition of acetic acid to the suspension of the 100% alumina layer. The induced roughness and surface porosity of the outer alumina layer should help in the osseointegration of the implant to the bone [4, 9, 14, 15]. Compressive strength was performed for the sintered FGM specimen and the average of three measurements was 166 MPa, which is more than that of Ti/HAp FGM (88 MPa) and TiN/HAp FGM (100 MPa) [20].



Figure 3: An optical image of the sintered FGM showing no cracks or separation of layers; the outer diameter is 3.2 mm and the thickness is  $900 \ \mu m$ 

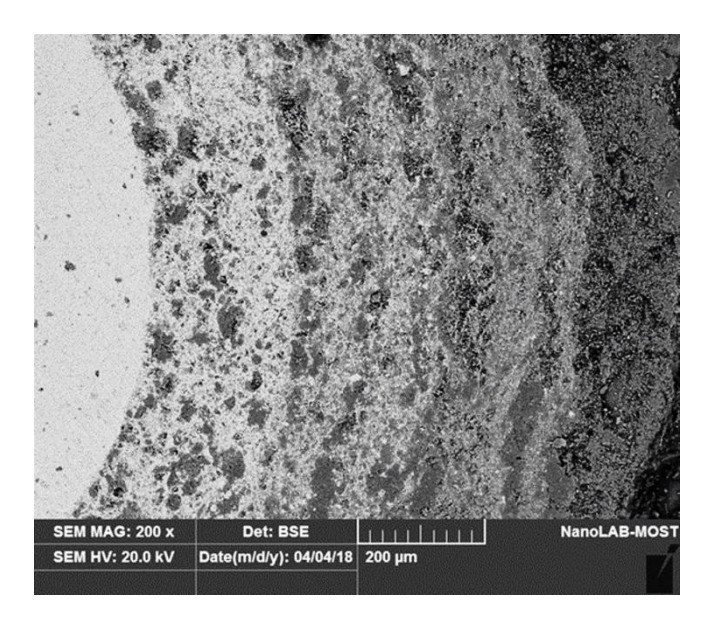


Figure (4): The zirconia-alumina gradation of the polished cross-section of the sintered FGM; the bright inner region is the zirconia and the darker outer region is the alumina

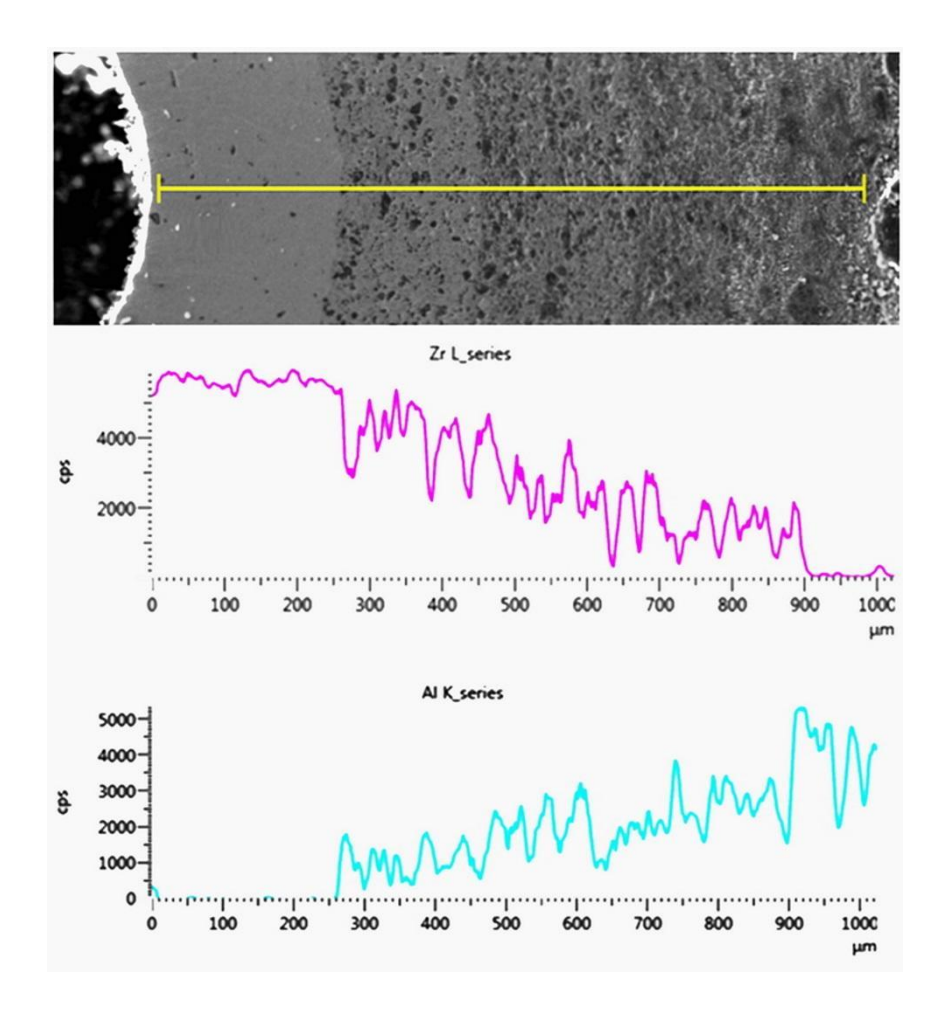


Figure 5: EDX line scans to the cross-section plane of the sintered FGM  $\,$ 

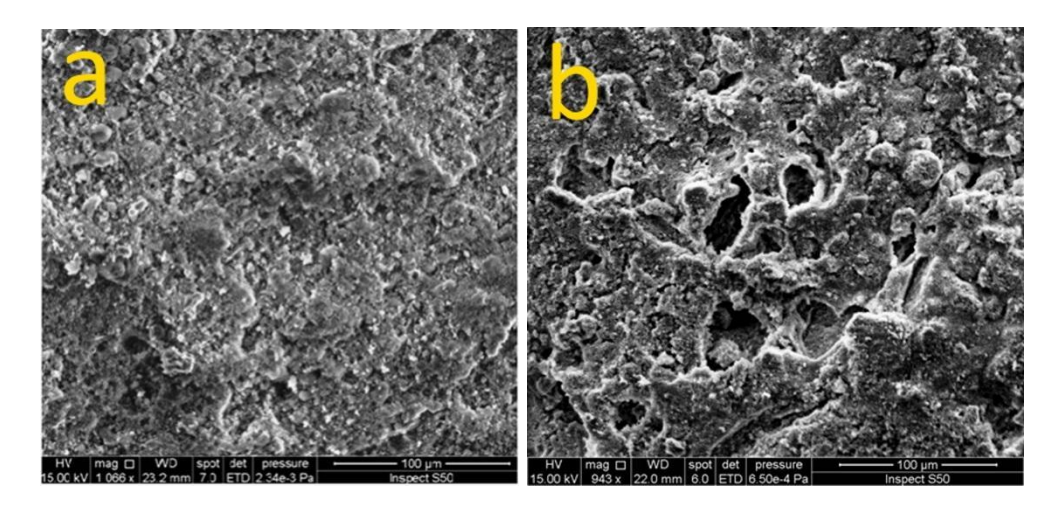


Figure 6: (a) The outer alumina surface of the sintered FGM without the addition of acid to the suspension; (b) Surface with the addition of acetic acid

Histological tests of the bone-implant interface via the H&E staining technique show no evidence of immunological or inflammatory response. Furthermore, there is no necrosis (death of cells) or alterations that would suggest the rejection of the material (Figures 7–12). Figure 7 indicates the formation of the trabeculae (connective) tissue at three weeks post-implantation, revealing the start of the reversal line. The osteocytes (bone cells) fill the trabeculae and the osteoblasts (bone-building cells) surround it (Figures 8–9).

A mature new bone surrounding the implant surface appeared at six weeks post-implantation (Figure 10). A lamellated mature bone is validated by the presence of the circular arrangements of osteocytes around the Haversian canals (tiny tubes that contain blood vessels), as seen in Figure 11. The osteocytes, the reversal line and the Haversian canals are more obvious in the closer view presented in Figure 12. Thus, the biocompatibility of the FGM implant is proven via the absence of implant rejection signs and the normal growth of new bone tissue in the implant–bone interface, signifying osseointegration. The development of the Haversian canal system indicates the advantage of the intended roughness and surface porosity of the outer layer of the implant. Thus, this synthesis is suggested as a dental implant for its biocompatibility and osseointegration.

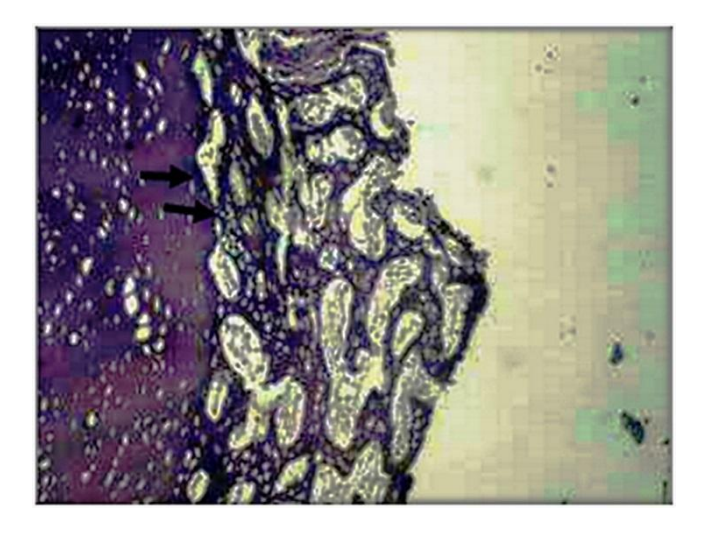


Figure (7): Histological view after three weeks shows new bone formation surrounding the implant surface (bright area on the left); a reversal line (black arrows) separates the old and new bone; H&E stain × 4

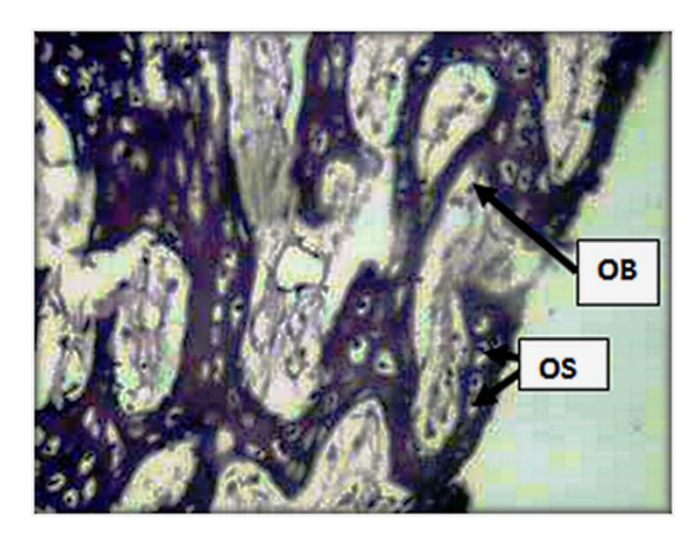


Figure (8): Higher magnification of three weeks post-implant shows new bone trabeculae filled with osteocytes (OS), bordered by osteoblasts (OB); H&E stain  $\times$  10

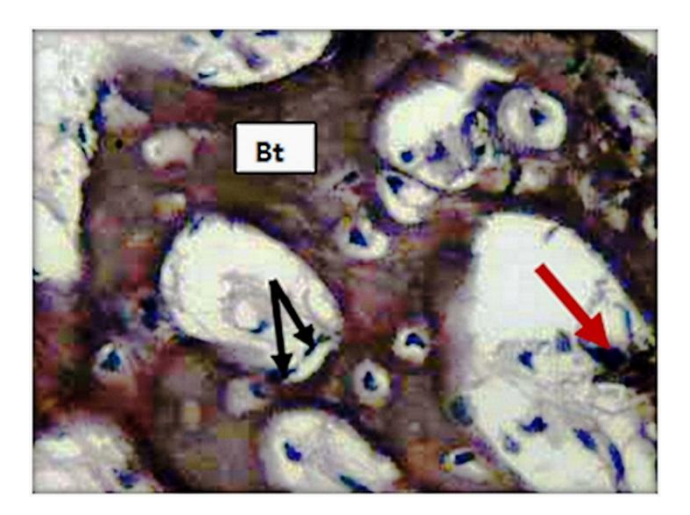


Figure (9): Histological view after three weeks shows new bone trabeculae (Bt), osteoblasts (black arrows) and osteoclasts (red arrow); H&E stain  $\times$  20



Figure (10): Histological view after six weeks shows mature new bone surrounding the implant surface, separated from the old bone by the reversal line (white arrows); H&E stain  $\times$  10

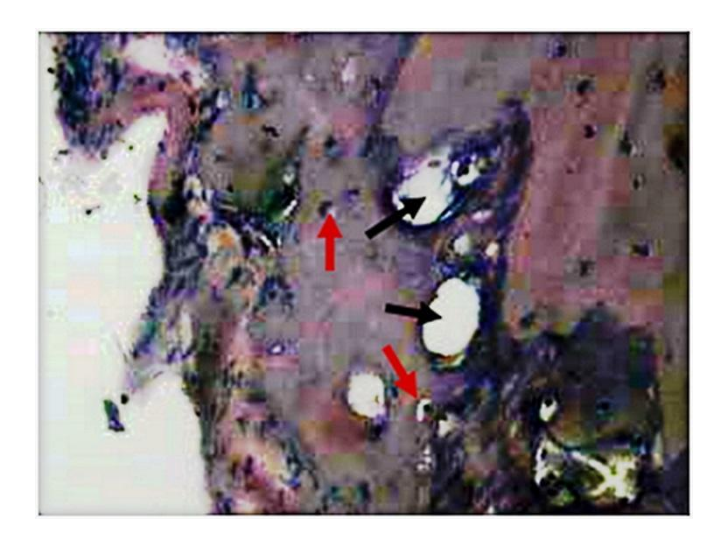


Figure (11): Higher magnification of the implant after six weeks shows lamellate mature bones by the presence of the circular arrangements of osteocytes (red arrows) around the Haversian canal (black arrows); H&E stain × 20

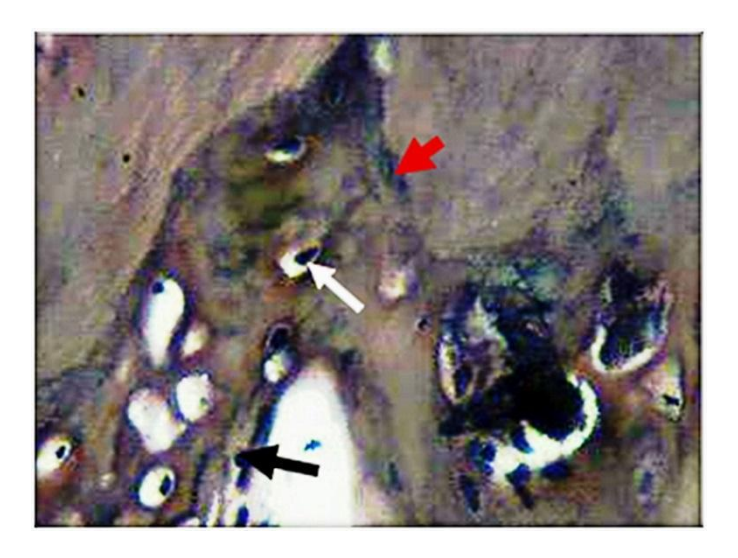


Figure (12): A closer view of the six-week bone-implant interface that shows mature new bone, which is demarcated from old bone by the reversal line (red arrow), filled with small size osteocytes (white arrow) and Haversian canals lined by osteoblasts (black arrow); H&E stain × 40

# 4. Conclusion

The EPD process was successfully utilised for the synthesis of integrated Zirconia–alumina cylindrical FGM with the noticeable roughness and surface porosity of the outer alumina layer. A unique set of suspension solutions was developed for the EPD process, which was based on polyethylene glycol. This was along with the utilisation of unique graded deposition voltages. Biocompatibility and osseointegration were proved via implantation in rabbit tibial bone and performing histological tests that revealed new bone formation and Haversian canals at the implant-bone interface.

# **Conflicts of Interest**

The authors declare no conflict of interest.

### References

- [1] J. Park and R. S. Lakes, *Biomaterials: an introduction*. Springer Science & Business Media, 2007.
- [2] M. Esposito, Y. Ardebili, and H. V. Worthington, "Interventions for replacing missing teeth: different types of dental implants," *Cochrane database of systematic reviews*, no. 7, 2014.
- [3] W. Höland *et al.*, "Future perspectives of biomaterials for dental restoration," *Journal of the European Ceramic Society*, vol. 29, no. 7, pp. 1291-1297, 2009.
- [4] J. J. Klawitter, A. M. Weinstein, F. W. Cooke, L. J. Peterson, B. M. Pennel, and R. V. Mckinney jr, "An evaluation of porous alumina ceramic dental implants," *Journal of dental research*, vol. 56, no. 7, pp. 768-776, 1977.

- [5] H. Kawahara, M. Hirabayashi, and T. Shikita, "Single crystal alumina for dental implants and bone screws," *Journal of Biomedical Materials Research*, vol. 14, no. 5, pp. 597-605, 1980.
- [6] T. Vajda, "Twelve Years' Clinical Experience with Single Crystal Alumina (Bioceramic) Dental Implants," in *Materials Science Forum*, 1988, vol. 34, pp. 379-385: Trans Tech Publ.
- [7] H.-C. Ko, J.-S. Han, M. Bächle, J.-H. Jang, S.-W. Shin, and D.-J. Kim, "Initial osteoblast-like cell response to pure titanium and zirconia/alumina ceramics," *Dental Materials*, vol. 23, no. 11, pp. 1349-1355, 2007.
- [8] W. Höland, M. Schweiger, R. Watzke, A. Peschke, and H. Kappert, "Ceramics as biomaterials for dental restoration," *Expert review of medical devices*, vol. 5, no. 6, pp. 729-745, 2008.
- [9] I. Denry and J. A. Holloway, "Ceramics for dental applications: a review," *Materials*, vol. 3, no. 1, pp. 351-368, 2010.
- [10] J. Ong, M. R. Appleford, and G. Mani, *Introduction to biomaterials: basic theory with engineering applications*. Cambridge University Press, 2014.
- [11] F. Mussano, T. Genova, L. Munaron, M. G. Faga, and S. Carossa, "Ceramic biomaterials for dental implants: Current use and future perspectives," *Dental Implantology and Biomaterial, 2nd ed.; Almasri, MA, Ed,* pp. 63-90, 2016.
- [12] I. V. Antoniac, Handbook of bioceramics and biocomposites. Springer Berlin, Germany:, 2016.
- [13] M. Malik, D. Puleo, R. Bizios, and R. Doremus, "Osteoblasts on hydroxyapatite, alumina and bone surfaces in vitro; morphology during the first 2 h of attachment," *Biomaterials,* vol. 13, no. 2, pp. 123-128, 1992.
- [14] G. Thompson, "Porous anodic alumina: fabrication, characterization and applications," *Thin solid films,* vol. 297, no. 1-2, pp. 192-201, 1997.
- [15] T. J. Webster, R. W. Siegel, and R. Bizios, "Nanoceramic surface roughness enhances osteoblast and osteoclast functions for improved orthopaedic/dental implant efficacy," *Scripta Materialia*, vol. 44, no. 8-9, pp. 1639-1642, 2001.
- [16] P. Christel, A. Meunier, M. Heller, J. Torre, and C. Peille, "Mechanical properties and short-term in vivo evaluation of yttrium-oxide-partially-stabilized zirconia," *Journal of biomedical materials research*, vol. 23, no. 1, pp. 45-61, 1989.
- [17] S. Deville, J. Chevalier, and L. Gremillard, "Influence of surface finish and residual stresses on the ageing sensitivity of biomedical grade zirconia," *Biomaterials*, vol. 27, no. 10, pp. 2186-2192, 2006.
- [18] B. Kieback, A. Neubrand, and H. Riedel, "Processing techniques for functionally graded materials," *Materials Science and Engineering: A*, vol. 362, no. 1-2, pp. 81-106, 2003.
- [19] C.-Y. Huang and Y.-L. Chen, "Design and impact resistant analysis of functionally graded Al203–Zr02 ceramic composite," *Materials & Design*, vol. 91, pp. 294-305, 2016.
- [20] M. Mehrali, F. S. Shirazi, M. Mehrali, H. S. C. Metselaar, N. A. B. Kadri, and N. A. A. Osman, "Dental implants from functionally graded materials," *Journal of Biomedical Materials Research Part A: An Official Journal of The Society for Biomaterials, The Japanese Society for Biomaterials, and The Australian Society for Biomaterials and the Korean Society for Biomaterials,* vol. 101, no. 10, pp. 3046-3057, 2013.
- [21] S. Put, J. Vleugels, and O. Van der Biest, "Gradient profile prediction in functionally graded materials processed by electrophoretic deposition," *Acta Materialia*, vol. 51, no. 20, pp. 6303-6317, 2003.
- [22] G. Anné, K. Vanmeensel, J. Vleugels, and O. Van der Biest, "Electrophoretic deposition as a novel near net shaping technique for functionally graded biomaterials," in *Materials Science Forum*, 2005, vol. 492, pp. 213-218: Trans Tech Publ.
- [23] L. Besra and M. Liu, "A review on fundamentals and applications of electrophoretic deposition (EPD)," *Progress in materials science*, vol. 52, no. 1, pp. 1-61, 2007.
- [24] G. Anné, S. Hecht-Mijic, H. Richter, O. Van der Biest, and J. Vleugels, "Strength and residual stresses of functionally graded Al2O3/ZrO2 discs prepared by electrophoretic deposition," *Scripta Materialia*, vol. 54, no. 12, pp. 2053-2056, 2006.
- [25] M. Mehrali, H. Wakily, and I. Metselaar, "Residual stress and mechanical properties of Al2O3/ZrO2 functionally graded material prepared by EPD from 2-butanone based suspension," *Advances in Applied Ceramics*, vol. 110, no. 1, pp. 35-40, 2011.
- [26] E. Askari, M. Mehrali, I. Metselaar, N. A. Kadri, and M. M. Rahman, "Fabrication and mechanical properties of Al2O3/SiC/ZrO2 functionally graded material by electrophoretic deposition," *Journal of the mechanical behavior of biomedical materials*, vol. 12, pp. 144-150, 2012.
- [27] A. Boccaccini, S. Keim, R. Ma, Y. Li, and I. Zhitomirsky, "Electrophoretic deposition of biomaterials," *Journal of the Royal Society Interface*, vol. 7, no. suppl\_5, pp. S581-S613, 2010.
- [28] I. Corni, M. P. Ryan, and A. R. Boccaccini, "Electrophoretic deposition: From traditional ceramics to nanotechnology," *Journal of the European Ceramic Society*, vol. 28, no. 7, pp. 1353-1367, 2008.
- [29] A. R. BOCCACCINI *et al.*, "The electrophoretic deposition of inorganic nanoscaled materials-a review," *Journal of the Ceramic Society of Japan*, vol. 114, no. 1325, pp. 1-14, 2006.
- [30] S. Lavenus, G. Louarn, and P. Layrolle, "Nanotechnology and dental implants," *International journal of biomaterials*, vol. 2010, 2010.

- [31] A. P. Tomsia, J. S. Lee, U. G. Wegst, and E. Saiz, "Nanotechnology for dental implants," *Oral & Craniofacial Tissue Engineering*, vol. 2, no. 1, 2012.
- [32] G. Thrivikraman, G. Madras, and B. Basu, "In vitro/in vivo assessment and mechanisms of toxicity of bioceramic materials and its wear particulates," *RSC Advances*, vol. 4, no. 25, pp. 12763-12781, 2014.
- [33] A. B. Novaes Jr, S. L. S. d. Souza, R. R. M. d. Barros, K. K. Y. Pereira, G. Iezzi, and A. Piattelli, "Influence of implant surfaces on osseointegration," *Brazilian dental journal*, vol. 21, no. 6, pp. 471-481, 2010.
- [34] B. Vidal et al., "Bone histomorphometry revisited," Acta Reumatologica Portuguesa, pp. 294-300, 2012.
- [35] P. Amrollahi, J. S. Krasinski, R. Vaidyanathan, L. Tayebi, and D. Vashaee, "Electrophoretic deposition (EPD): Fundamentals and applications from nano-to micro-scale structures," *Handbook of Nanoelectrochemistry, Springer International Publishing Switzerland*, 2015.
- [36] I. Smallwood, Handbook of organic solvent properties. Butterworth-Heinemann, 2012.
- [37] S. K. Loghmani, M. Farrokhi-Rad, and T. Shahrabi, "Effect of polyethylene glycol on the electrophoretic deposition of hydroxyapatite nanoparticles in isopropanol," *Ceramics International*, vol. 39, no. 6, pp. 7043-7051, 2013.
- [38] W. Chartarrayawadee, S. E. Moulton, C. O. Too, and G. G. Wallace, "Fabrication of graphene electrodes by electrophoretic deposition and their synergistic effects with PEDOT and platinum," 2013.
- [39] J.-C. M'Peko, D. L. Spavieri, C. L. da Silva, C. A. Fortulan, D. P. F. de Souza, and M. F. de Souza, "Electrical properties of zirconia–alumina composites," *Solid State Ionics*, vol. 156, no. 1, pp. 59-69, 2003/01/01/2003.



© 2020 by the authors. Licensee Ziggurat Publishing, London, United Kingdom. This article is an open access article distributed under the terms and conditions of the Creative Commons Attribution (CC BY) license (http://creativecommons.org/licenses/by/4.0)